Microporous and Mesoporous Materials 164 (2012) 273–279

Contents lists available at SciVerse ScienceDirect

Microporous and Mesoporous Materials

journal homepage: www.elsevier.com/locate/micromeso

Exploring the hierarchy of transport phenomena in hierarchical pore systems by NMR diffusion measurement

Dirk Mehlhorn [a], Rustem Valiullin [a], Jörg Kärger [a,*], Kanghee Cho [b], Ryong Ryoo [b]

[a] Faculty of Physics and Earth Science, University of Leipzig, Linnéstr. 5, Leipzig D-04103, Germany
[b] Department of Chemistry and Graduate School of Nanoscience and Technology (WCU), KAIST, Daejeon 305-701, Republic of Korea

ARTICLE INFO

Article history:
Available online 7 July 2012

Dedicated to Prof. Dr. Jens Weitkamp on the occasion of his 70th birthday

Keywords:
Mesoporous zeolites
LTA
Diffusion
Hierarchical pore systems
Pulsed field gradient NMR

ABSTRACT

The pulsed field gradient technique of NMR (PFG NMR) is applied for exploring molecular diffusion in different specimens of zeolite NaCaA, notably in samples containing "hierarchical" pore systems where the micropores are traversed by mesopores. Choosing ethane (capable of permeating both micro- and mesopores) and cyclohexane (unable to penetrate the micropores) as guest molecules and varying purposefully the accessibility and mobility in the mesopores by temperature variation and pore blocking, the diffusivities in the two pore spaces are measured separately from each other. It is shown that the presence of the mesopores may give rise to dramatically enhanced intracrystalline diffusivities while a blockage of the mesopores reduces the intracrystalline diffusivities by an order of magnitude.

1. Introduction

In the middle of the last century, the introduction of nanoporous materials has revolutionized the technologies for product upgrading by mass separation [1] and mass conversion [2]. The worldwide annual benefit attained by such technologies in, e.g., only petrol refining is estimated to be of the order of 10 billion Euros [3]. With groundbreaking investigations in the field of heterogeneous catalysis [4], Jens Weitkamp has notably contributed to this impressive development. We dedicate this paper to him on the occasion of his 70th birthday, in appreciation of these contributions and in gratitude for many stimulating advices for our own work.

In the last few years, the requirement for sustainable, energy efficient and clean technologies has given rise to new orientations and developments in the fabrication, investigation and application of nanoporous materials. A substantial amount of these studies is dedicated to the solution of a problem inherent to the application of nanoporous materials quite in general: Their great potentials in shape-selective catalysis [2–4] and mass separation by molecular sieving and selective adsorption [1] results from the intimate contact between the guest molecules and the host surfaces, notably by choosing pore sizes as close as possible to the sizes of the involved molecules. One has to pay for this closeness with, in general, dramatically reduced guest diffusivities [5–8]. The gain in value-added products by molecular conversion or separation, however, can never exceed the relevant diffusion rates [8,9]. The closeness between molecular and pore sizes which, on the one hand side, is the prerequisite for the elementary processes leading to the desired processes, is thus found, on the other side, to limit their performance.

Among the various strategies developed for overcoming this dilemma, the fabrication of materials with hierarchical pore spaces has attracted particular attention. In such materials, a microporous (in general zeolitic) bulk phase, the "source" of the value-added products, is traversed by (or embedded in) a network of mesopores, the product of the relative micropore volume (V_{micro}/V_{total}) and the relative mesopore surface area (S_{meso}/S_{BET}) being known as the hierarchy factor [10]. The techniques applied in the fabrication of such "mesoporous" zeolites include "hard" [11] and "soft" (supramolecular) [12–15] templating methods as well as post-synthetic dealumination or desilication [16–18].

It is well known that, due to huge differences in the results of different measuring techniques, the diffusivity in purely microporous materials remained, over decades, a mystery [19,20]. Only recently, owing to the combined application of "microscopic" techniques of diffusion measurement [8], notably Quasi-Elastic Neutron Scattering [21], pulsed field gradient NMR (PFG NMR) [22,23] and micro-imaging by IR and interference microscopy [24], the differences in the diffusivities obtained by different techniques could be referred to the influence of transport resistances

* Corresponding author.
E-mail address: kaerger@physik.uni-leipzig.de (J. Kärger).

1387-1811/$ - see front matter © 2012 Elsevier Inc. All rights reserved.
http://dx.doi.org/10.1016/j.micromeso.2012.06.049

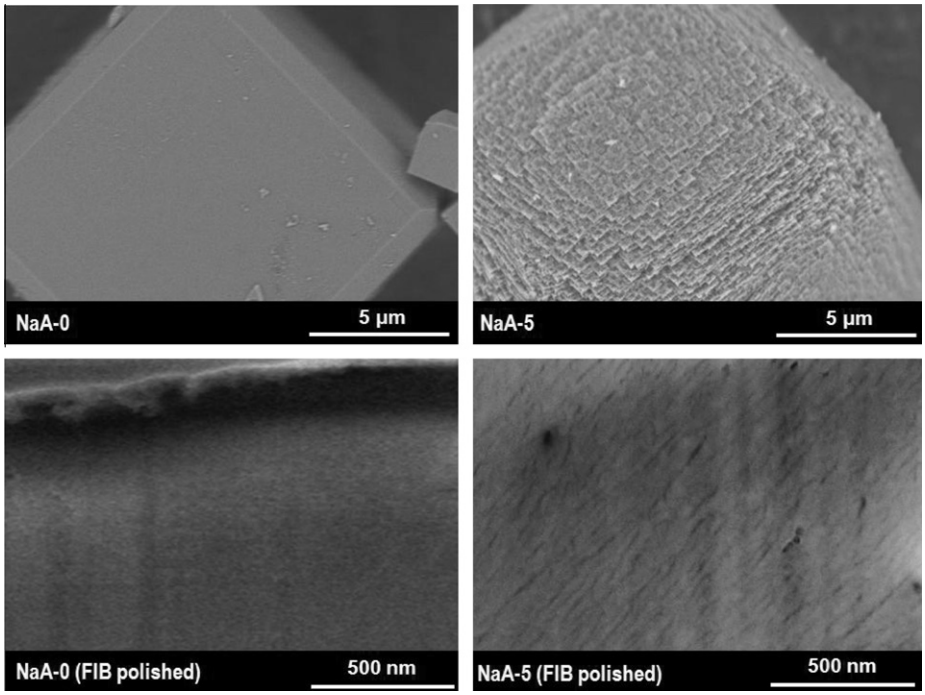

Fig. 1. SEM images of the purely microporous (NaA-0, left column) and a mesoporous (NaA-5, right column) LTA zeolite sample: top images were taken from the external surfaces of the calcined samples and the bottom images were taken after cross-sectional polishing by focused gallium ion beam. The dark, slant lines in the lower right image indicate the presence of mesopores in the cross-sectional cut.

acting in addition to the genuine pore structure which appear to be essentially omnipresent in the "real" structure of nanoporous materials [25,26]. A clear separation between the influences of these different types of transport resistances remains a challenging task of current diffusion research.

Similarly challenging is the situation with hierarchical pore systems. It is not unexpected, therefore, that first diffusion studies with mesoporous zeolites were only focused on the combined effect of the two pore systems on the rates of molecular uptake and intracrystalline molecular diffusion, including macroscopic uptake experiments [27] and microscopic diffusion measurements by PFG NMR [28–30]. In the present communication, we report about first PFG NMR diffusion studies aiming at a separate determination of the diffusion properties of the micro- and mesoporous spaces in zeolites with a hierarchical pore system.

2. Experimental

2.1. The material under study

The measurements have been performed with three specimens of calcium-exchanged zeolite LTA, one purely microporous (NaCaA-0) and two mesoporous ones with mesopore volumes of 0.110 cm^3/g (NaCaA-2) and 0.218 cm^3/g (NaCaA-5), respectively. The width of the mesopores is estimated to be about 5 nm. The SEM pictures shown in Fig. 1 provide an impression of their morphology.

Following the procedure described in detail in Ref. [31], the mesoporous zeolite LTA was synthesized under the presence of 3-(trimethoxysilyl)propylhexadecyldimethylammonium chloride (TPHAC) as an organosilane surfactant, giving rise to the formation of mesopores within the LTA microporous space. The numbers following 'Na(Ca)A-' in the sample names mean the mole percent of organosilane surfactant to entire silica species (silicate + organosilane) in the initial synthetic gel. Finally, 82% of the sodium ions were replaced by Ca2+ cation exchange.

Ref. [29] provides a summary of the results of previous PFG NMR diffusion studies of this material with propane as a guest molecule as well as further details of sample preparation and characterization. It was in particular confirmed that morphology, particle size and external/internal mesopore structure of all samples are maintained after calcination and ion-exchange treatments. In all samples, the mean crystal diameter was about 11 µm and proved to be big enough for allowing PFG NMR diffusion studies free of disturbing boundary effects.

2.2. PFG NMR diffusion measurements

Under the influence of a pair of field gradient pulses, applied in addition to the sequence of radio-frequency pulses giving rise to the formation of the NMR signal ("spin echo" of intensity M), signal attenuation obeys the relation [23,32,33]

$$M(\delta g)/M(0) \equiv \psi(\gamma\delta g, t) = \int_{-\infty}^{\infty} P(z,t)\cos(\gamma\delta g z)dz \qquad (1)$$

with g and δ denoting, respectively, the amplitude and duration of the gradient pulses. t stands for the observation time of the PFG NMR experiment, i.e., the time interval between the two gradient pulses (where, for simplicity, the pulse width δ is implied to be negligibly small in comparison with t). $\gamma(=2.67\times10^8\ T^{-1}\ s^{-1}$ for protons) is the gyromagnetic ratio. $P(z, t)$ denotes the probability that, during time t, an arbitrarily selected molecule within the sample is shifted over a distance z, i.e., in the direction of the applied field gradient. This interrelation between the signal attenuation curve $\psi(\gamma\delta g, t)$ and the "mean propagator" $P(z, t)$ [23,32–34] gives rise to the matchless versatility of PFG NMR for the exploration of molecular mass transfer in complex systems which, in this study, shall be exploited for an in-depth study of mass transfer in the two pore systems of mesoporous zeolites.

For molecules in an infinitely extended, isotropic medium the propagator is a Gaussian [8]

$$P(z,t) = \frac{1}{\sqrt{4\pi Dt}} \exp\left\{-\frac{z^2}{4Dt}\right\} \quad (2)$$

with the mean square width (molecular mean square displacement) given by the Einstein formula [35]

$$\langle z^2(t)\rangle = \int_{-\infty}^{\infty} z^2 P(z,t)dz = 2Dt \quad (3)$$

with the self-diffusivity D. Under conditions where Eqs. (2) and (3) are applicable, the molecules are said to undergo "normal" diffusion. As a mean prerequisite of normal diffusion, the probability of molecular propagation has to be independent of the past. Important examples for deviations from this behavior, i.e. for the occurrence of "anomalous" diffusion, include diffusion in fractal pore networks [36,37] and "single-file" diffusion [38], where there is a bias on molecular propagation back to its origin. Such deviations become only relevant if, over the total diffusion path length, pore architecture totally adheres to the structural requirements of fractal geometry and of single-file diffusion, respectively. Due to the omnipresence of structural defects [21–26], real porous systems are known to generally deviate from such ideality so that, for diffusion path lengths in the range of micrometres, i.e. notably larger than the usual distances between such defects (but still much smaller than the particle diameters), normal diffusion and, hence, Eqs. (2) and (3) may be implied to hold quite generally.

The importance of the information provided by PFG NMR for evaluating mass transfer phenomena during separation and conversion may be rationalized by realizing that, completely equivalently with Eq. (3), the self-diffusivity may also be defined, following Fick's 1st diffusion law, as the factor of proportionality between diffusion fluxes and concentration gradients

$$J^* = -D\nabla c^* \quad (4)$$

It is indicated by the asterisks that it is the flux and the concentration of *labelled* molecules under equilibrium conditions (rather than the total flux and concentration under the (non-equilibrium) conditions of transport-diffusion measurements) which is here considered. The diffusivity of labelled molecules (of "tracers") does clearly serve as an excellent "spy" exploring the mobility of the respective molecular species under the given conditions of technological application [39] and does, moreover, even coincide with the relevant (transport) diffusivity in the limit of sufficiently small concentrations [23].

With Eqs. (2) and (3) one obtains, from Eq. (1),

$$\psi(\gamma\delta g,t) = \exp\{-\gamma^2\delta^2 g^2 Dt\} = \exp\left\{-\frac{1}{2}\gamma^2\delta^2 g^2\langle z^2(t)\rangle\right\} \quad (5)$$

The second relation provides a reasonable approach also under such conditions, where Eqs. (2) and (3) are not valid anymore. In such cases, it is useful to maintain Eq. (3), now, however, with the understanding that the thus defined diffusivity is but an apparent (or effective) one rather than a genuine ("microscopic") diffusivity. In the limiting case of sufficiently large observation times for molecular displacements confined to a sphere of radius R (considered as an approximation for the shape of an individual zeolite crystal), the thus defined effective diffusivity, e.g., results to be [8,23]

$$D_{restr.} = \frac{R^2}{5t} \quad (6)$$

If, during the observation time t of the PFG NMR experiment, a notable fraction of the guest molecules is able to exchange between different adsorbent particles, the PFG NMR attenuation curve becomes a linear combination of two exponentials of the form of Eq. (5)

$$\psi(\gamma\delta g,t) = p(t)\exp\left\{-\frac{1}{2}\gamma^2\delta^2 g^2\langle z^2(t)\rangle_{intra}\right\} + (1-p(t))\exp\left\{-\frac{1}{2}\gamma^2\delta^2 g^2\langle z^2(t)\rangle_{long-range}\right\} \quad (7)$$

where now (only) the first term stands for diffusion inside the crystals (intracrystalline diffusion) while the second term refers to diffusion and molecular exchange through the external space (long-range diffusion). The function $p(t)$ denotes the fraction of molecules which, during the observation time t, have remained within one and the same crystal.

The PFG NMR measurements of this study were performed with the so-called 13-interval stimulated-echo pulse sequence [40]. In this technique possibly disturbing influences by internal field gradients are further reduced by replacing the two field gradient pulses of the basic experiment by pairs of pulses with opposite field gradient amplitudes, separated by an rf pulse (the "π-pulse"). In our measurements, we have used the home-built PFG NMR spectrometer FEGRIS 400 operating at proton resonance with a frequency of 400 MHz, offering a maximum field gradient intensity of 35 Tm^{-1} [41,42]. Typical values of the gradient pulse width δ and the observation time t were 0.3–1.0 ms and 5–80 ms, respectively. Temperature was varied from about −110 °C up to + 60 °C by means of evaporating liquid nitrogen below and with preheated air above room temperature, attaining an accuracy of about ± 1 K.

Prior to the PFG NMR diffusion measurements, the zeolite material was introduced into glass tubes of 7 mm diameter with a filling height of 10 mm. Under continuous evacuation, the tubes were heated at a rate of 10 K h^{-1} to 673 K. After keeping them at this temperature for about 12 h and cooling down, under continued evacuation, the guest molecules (ethane or/and cyclohexane) were introduced by means of liquid nitrogen from a calibrated volume under a well-defined pressure. For ethane, the loadings corresponded to 3 molecules per supercage of the micropore structure. The amounts of cyclohexane were chosen to correspond to the total mesopore volume of the samples. In the samples with both ethane and cyclohexane, cyclohexane was applied in the deuterated form. In this way, only the ethane molecules, whose diffusivities we were interested in, gave rise to the observed ^{1}H NMR signal. After loading, the sample tubes were closed hermetically. Equilibration of the guest molecules within the sample was confirmed by a repetition of the measurements over a time span of several weeks, which yielded completely coinciding results.

3. Results and discussion

3.1. The primary data of the PFG NMR diffusion experiments

Fig. 2a–c show examples of the primary data of the PFG NMR diffusion experiments, the PFG NMR signal attenuations, in three typical cases considered in this study, namely with ethane in the purely microporous sample (Fig. 2a), and with ethane (Fig. 2b) and cyclohexane (Fig. 2c) in a mesoporous sample. In all three cases one recognizes, notably for the largest observation times, the pattern of Eq. (7) with a first, fast decay corresponding to this part of the molecules which, during t, are able to leave the individual crystallites in which they have been at time $t = 0$. In complete agreement with our expectation, this part becomes more and more significant with increasing time, corresponding to a decrease in the relative amount $p(t)$ of guest molecules which, during the observation time t, have remained within one and the same crystal.

In this study, our interest is focused on mass transfer in the interior of the individual crystallites which is reflected by the second, more slowly decaying part of the attenuation curves. This part is seen to be accessible with highest accuracy at the smallest

observation times. Hence, in all our further discussion, we confine ourselves to the attenuation curves attained with $t = 10$ ms.

Deviating from the ideal behavior implied with Eqs. (5) and (7), the attenuation curves are seen to slightly deviate from a strict exponential dependence (where, in the semi-logarithmic plot, the curve has to become a straight line). Such deviations are a simple consequence of slight differences in the guest diffusivities in different crystals, with the mean value of these diffusivities determining the slope in the beginning of the attenuation curve [8]. It is this mean value which we are going to consider in this study.

Before, in the subsequent sections, the diffusion properties shall be discussed in more detail, we use the presentations of Fig. 2a–c for identifying some general features.

(i) In the limit of small observation times, in all three cases the slope of the attenuation curves ln ψ vs. $\gamma^2\delta^2g^2t$ is seen to remain invariant with increasing observation time. With Eq. (5) such a behavior is seen to indicate normal diffusion, i.e. a constant diffusivity or, with Eq. (3), correspondingly, molecular mean square displacements increasing linearly with time.

(ii) For the largest observation times, notably in Fig. 2a and b, the slope of the second part of the attenuation curves is seen to decrease with further increasing observation times. We thus easily recognize the conditions under which the system under study cannot be considered anymore to be infinitely extended. Decreasing slopes with increasing observation times are reflected by Eq. (6) where – in the limiting case of sufficiently large observation times – the effective diffusivity for intracrystalline displacements is seen to decrease in proportion with the increase of the observation time.

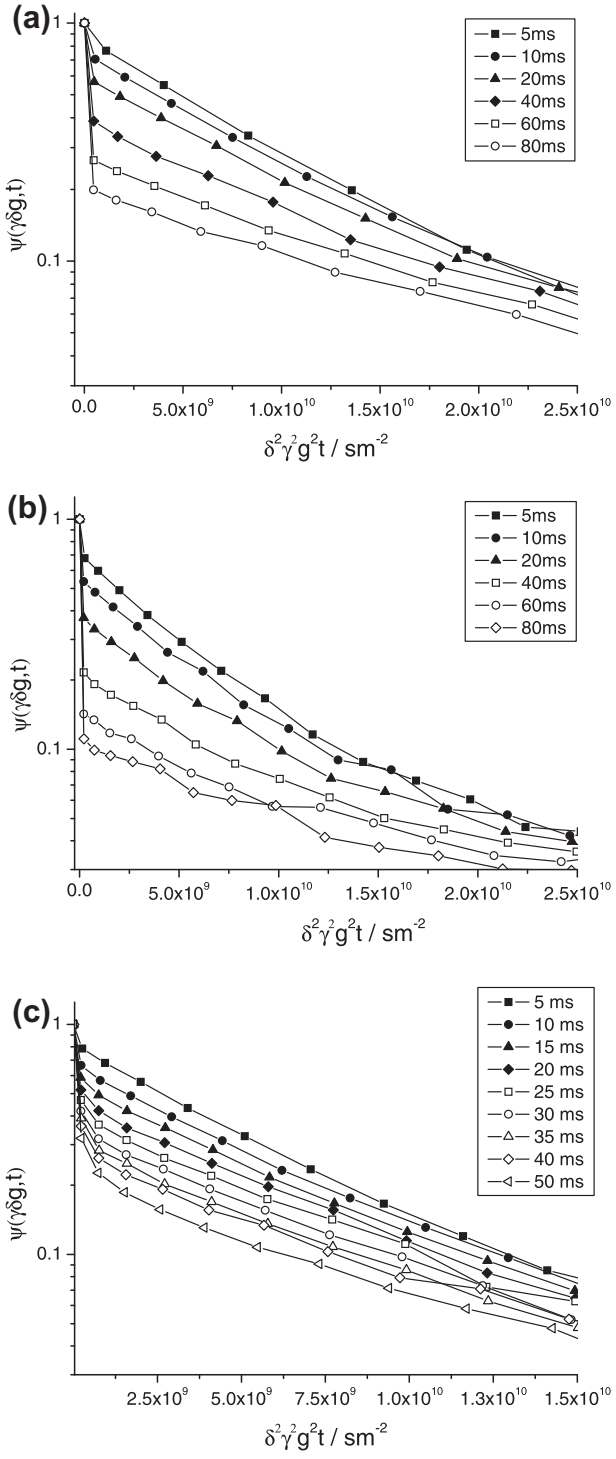

Fig. 2. PFG NMR signal attenuation curves with ethane in the purely microporous zeolite (NaCaA-0, (a)) and with ethane (b) and cyclohexane (c) in the mesoporous zeolite (NaCaA-5), recorded at 25 °C.

3.2. The ethane diffusivities: tracing micro- and mesopore spaces

Fig. 3 shows the ethane diffusivities measured in the purely microporous zeolite (NaCaA-0; open circles) and compares them with the diffusivities in the mesoporous zeolites NaCaA-2 (triangles) and NaCaA-5 (diamonds), both with ethane as the sole guest molecule (open symbols) and with additional deuterated cyclohexane saturating the mesopore space (filled symbols) over the temperature range from 164 up to 333 K considered in this study. The straight line connecting the diffusivities in the purely microporous zeolite is the best fit of the experimental data to the Arrhenius dependence $D_{NaCaA} = D_0 \exp(-E_D/RT)$, yielding an activation energy of $E_D = 6.3 \pm 0.3$ kJ/mol. Both the absolute value and the activation energy of intracrystalline diffusion are in accordance with the

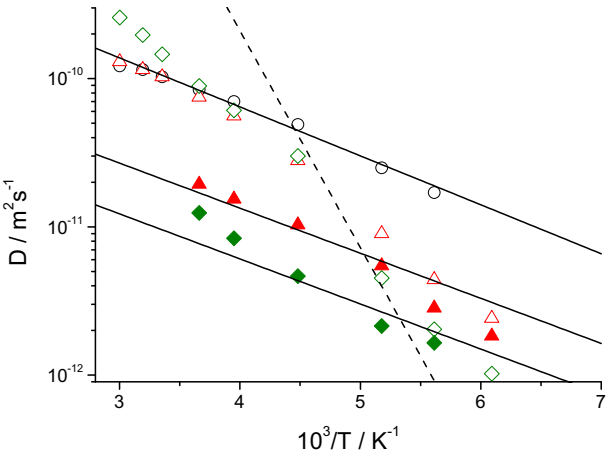

Fig. 3. Intracrystalline diffusivities of ethane in a purely microporous specimen of zeolite NaCaA (NaCaA-0, circles) and in mesoporous NaCaA (NaCaA-2, triangles and NaCaA-5, diamonds), both with only ethane adsorbed (open symbols) and with co-adsorbed cyclohexane, saturating the total mesopore volume (filled symbols). Full lines represent the best Arrhenius fit to the diffusivities in the purely microporous specimen and their parallel shifts to lower values, following Eq. (9) with the understanding that they represent estimates of the intracrystalline diffusivities with the mesopores representing "forbidden" regions for mass transfer. The broken line is a guide for the eyes representing the variation of the contribution of diffusion in the (unblocked) mesopores (Eq. (10)) to the overall intracrystalline diffusivity.

results of previous PFG NMR diffusion studies with purely microporous zeolites LTA [43].

A parallel shift of this line to lower values is found to approach the ethane diffusivities in the mesoporous zeolites if the mesopores are filled with cyclohexane. This is, in fact, exactly the behavior to be predicted on considering the different contributions to intracrystalline guest diffusion in mesoporous zeolites [23,29,44]. Under the assumption that there is fast molecular exchange between the meso- and micropore spaces, the intracrystalline diffusivity (as resulting from the second, slowly decaying part of the attenuation curves as discussed in Section 3.1) results as the superposition of the relative contributions due to displacements in the two pore spaces, yielding

$$D_{intra} = p_{micro}D_{micro} + p_{meso}D_{meso} \approx D_{micro} + p_{meso}D_{meso} \quad (8)$$

with $p_{\mathrm{micro(meso)}}$ and $D_{\mathrm{micro(meso)}}$ denoting, respectively, the relative amounts and the diffusivities of the guest molecules under study in the respective (micro- or meso-) pore spaces. In the second relation we have made use of the fact that, with ethane as a probe molecule, the guest concentrations in the micropores significantly exceeds those in the mesopores ($p_{\mathrm{micro}} \gg p_{\mathrm{meso}}$) so that, due to $p_{\mathrm{micro}} + p_{\mathrm{meso}} = 1$, one has $p_{\mathrm{micro}} = 1$. Using propane as a probe molecule, it has been illustrated in Ref. [29] by both experimental evidence and model calculation that, irrespective of the inequality in the population in the two pore spaces, the second term in Eq. (8) is able to lead to an orders-of-magnitude enhancement of the intracrystalline diffusivity of mesoporous zeolites in comparison with the intracrystalline diffusivity in the purely microporous specimen: As a consequence of the large mean free paths in the void space of the mesopores, giving rise to Knudsen-type molecular propagation [45,46], the diffusivity in the mesopores may easily exceed the micropore diffusivities by several orders of magnitude.

This option does not exist anymore in the samples with liquid-filled mesopores: The diffusivity of the ethane molecules which, dissolved in cyclohexane, populate the mesoporous space is now slowed down dramatically. Rather than accelerating intracrystalline mass transfer, the presence of mesopores is now giving rise to its decrease, caused by the necessity that now the mesopores are essentially circumscribed by the diffusing molecules. This is exactly the situation known from mass transfer in media containing "forbidden" regions. For diffusion path lengths notably exceeding the distances between these regions, the resulting diffusivity (D_{eff}) is known to be reduced by a constant factor in comparison with the diffusivity D_{bulk} in the unperturbed bulk phase [8,36,47–49]:

$$D_{eff} = D_{bulk}/\tau \quad (9)$$

with the "tortuosity" τ assuming, in pore spaces, values of typically 2 to 5. The tortuosity is known to increase, in general, with increasing volume fractions of the forbidden regions [8,49] so that it is not unexpected that the ethane diffusivities in the samples with a larger fraction of blocked mesopores are distinctly below those with the smaller content of mesopores.

It is interesting to note that, with varying temperature, the ethane diffusivities in the mesoporous samples with "unblocked" mesopores are able to follow both patterns of influence of the mesopores on the overall diffusivities, i.e. to give rise to both acceleration and deceleration of diffusion in comparison with diffusion in the genuine microporous bulk phase. This is the direct consequence of the fact that, being proportional to the ethane pressure in the closed PFG NMR samples, the fraction p_{meso} of ethane molecules follows an Arrhenius dependence

$$P_{meso} \sim \exp(-E_{ads}/RT) \quad (10)$$

with E_{ads} denoting the isosteric heat of adsorption [8,29]. This relation is indicated by the broken line in Fig. 3 (with a value of $E_{\mathrm{ads}} = 28$ kJ/mol as taken from Ref. [50]) and illustrates the relative contribution of the second term in Eq. (8) (given the fact that, being proportional to the square root of the temperature, the value of D_{meso} does not vary significantly over the temperature range considered in our experiments).

Correspondingly, for high temperatures the slope of the Arrhenius plots of the ethane diffusivities in the unblocked mesoporous zeolites is seen to approach that of the broken line. In the limit of sufficiently low temperatures, on the other side, the contribution of mesopore diffusion becomes negligibly small so that the diffusivities in the zeolites with unblocked mesopores approach those in the zeolites with blocked mesopores.

For rationalizing the temperature dependence of the ethane diffusivity in the mesoporous zeolites, notably in NaCaA-5, one should have in mind that, with varying temperature, there is also a change in the microdynamic conditions under which the "micropore diffusivity" D_{micro} appearing in Eq. (8) is determined. On encountering the surface of the microporous space, with decreasing temperature more and more guest molecules will fail to get into the free space. This is the immediate consequence of the decrease in thermal energy which as well appears in the decreasing equilibrium pressure in the surrounding atmosphere. Molecular displacements towards the surface, notably towards the internal one formed by the mesopores, will thus be followed predominantly by displacements back into the range of the micropores. Therefore, both displacements tend to compensate each other, leading to mean square displacements and, with Eq. (3), to diffusivities notably reduced in comparison with the purely microporous zeolites. This effect fades away with increasing temperature [51]. The experimentally observed steep increase in the ethane diffusivities in NaCaA-2 and -5 with increasing temperature (Fig. 3) must therefore be attributed to an increase in the contribution of mesopore diffusion as well as to an increase in the micropore diffusivities due to reduced anti-correlations in molecular displacement (acting in addition to the normal Arrhenius dependence).

The effect of anti-correlations in molecular displacements is automatically taken account of in the series-parallel formulae of diffusion in heterogeneous media [52]. In the given context, it may be noted in the form

$$D_{intra} = p_1 D_{micro} + p_2 p_{meso} D_{meso} + p_3 \frac{D_{micro} p_{meso} D_{meso}}{D_{micro} + p_{meso} D_{meso}} \quad (11)$$

This approach takes into account that, within the hierarchical pore space, there are essentially three different types of diffusion paths for the guest molecules within the individual crystals of mesoporous zeolite, namely paths exclusively within the spaces of either the micro- or the mesopores or paths through both spaces where the mesopores may be imagined as "interruptions" in a continuous space of micropores. As the most simple approach, Eq. (11) has been chosen as a linear combination of these three mechanisms. All mechanisms are thus considered to operate in parallel, with the last term resulting from a series arrangement of the diffusivities in the micro- and mesopores. The prefactor p_{meso} takes account of the difference in the equilibrium concentrations in the two pore spaces (see, e.g., Section 15.8.1 in Ref. [8]).

Since the heat of adsorption can be expected to notably exceed all other activation energies, the temperature dependence of Eq. (11) is determined by that of p_{meso} and, with Eqs. (10) and (11), we may easily identify two limiting cases, namely for

$$-\text{high temperatures } (p_{meso}D_{meso} >> D_{micro}) : D_{intra} = p_2 p_{meso} D_{meso} \quad (12)$$

$$-\text{low temperatures } (p_{meso}D_{meso} << D_{micro}) : D_{intra} = p_1 D_{micro} + p_3 p_{meso} D_{meso} \quad (13)$$

With these equations, the ethane diffusivities in the mesoporous zeolites (with the mesopores left unblocked) can be nicely rationalized and referred to our model considerations: Even at

the highest temperatures considered in this study, the values of D_{intra} are still of the order of the micropore diffusivities. The conditions for the validity of Eq. (12) are in no way fulfilled therefore. It is hence in complete agreement with our expectation that the slope in the Arrhenius plot of the effective diffusivity of ethane in NaCaA-5 as shown in Fig. 3 is intermediate between those of p_{meso} (broken line) and D_{micro} (full lines). With Eq. (13) we note that, in the limit of small temperatures, D_{intra} drops with the decreasing contribution of $p_3\, p_{meso} D_{meso}$ to the level of micropore diffusion, impeded by the presence of the, then essentially inaccessible, mesopores. In this range, the decay of D_{intra} is seen to nicely follow that of p_{meso}, as expected.

3.3. Diffusion of cyclohexane: confinement to mesopores

The critical diameter of about 0.69 nm of the cyclohexane molecules notably exceeds the effective diameter of about 0.42 nm of the "windows" connecting the micropores ("large cavities") of zeolite NaCaA. It is unable, therefore, to enter the micropore space and intracrystalline diffusion in mesoporous LTA-type zeolites has to exclusively proceed within the space of the mesopores. We are thus confronted with a situation similar to the one just considered, however with an interchange of the parts of the two subspaces: It is now the diffusivity in the mesopores we are interested in, while the space of the micropores has become the "forbidden" region.

At room temperature, these diffusivities result to be $(1.0 \pm 0.1) \times 10^{-10}$ m^2 s^{-1} in NaCaA-2 and $(1.7 \pm 0.1) \times 10^{-10}$ m^2 s^{-1} in NaCaA-5. These values are about one order of magnitude below the diffusivities of cyclohexane in the free liquid phase 1.4×10^{-9} m^2 s^{-1} [53]. In addition to the influence of tortuosity, however, also the "friction" with the pore walls is known to contribute to such a reduction: Even in a straight channel of similar pore size, diffusion in axial direction is known to be reduced in comparison with the diffusivity in the free liquid by factors of typically 2–3.

With Fig. 2, molecular diffusion in both subspaces has been found to be normal, i.e. to give rise to mean square displacements increasing linearly with the observation time. Both subspaces, i.e. both the meso- and the micropores, could thus be demonstrated to form mutually interpenetrating spaces, in complete agreement with the evidence provided by the observation that platinum agglomeration in the mesopores leads to the formation of three-dimensional networks [31]. Normal diffusion in both subspaces was required already with noting Eq. (7) where the micro- and mesopore diffusivities were introduced as time-independent parameters by applying the Einstein relation, Eq. (3), for the respective pore spaces [51].

3.4. Pore space hierarchy and diffusivities

In our experiments, for one of the considered probe molecules (ethane) the mesopores could be made essentially inaccessible (by either blocking them with cyclohexane or by measurements at sufficiently low temperatures) while the second probe applied (cyclohexane) was chosen to be so bulky that it was unable to enter the micropores. In this way it has become possible to investigate separately the diffusion behavior in two spaces which are exactly complementary to each other. For correlating the respective diffusivities, Fig. 4 summarizes the relevant diffusion data of ethane (tracing the micropore subspace) and of cyclohexane (tracing the mesopore subspace). The data points nicely reflect the expected tendency that the diffusivity in a given subspace decreases with the decrease of its volume fraction. Thus, the micropore diffusivity (as probed with ethane) in NaCaA-2 is found to be larger than in NaCaA-5, while exactly the opposite is true with the mesopore diffusivities as probed with cyclohexane.

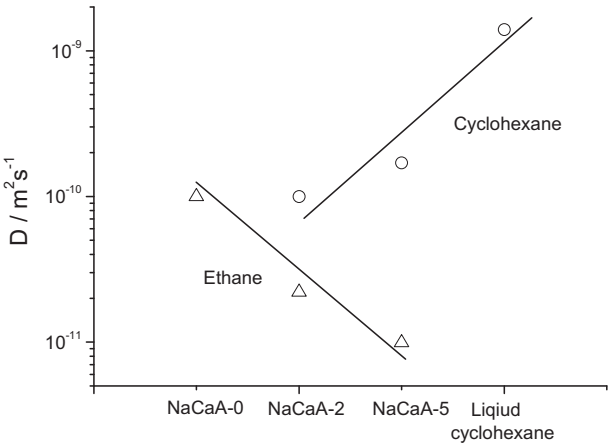

Fig. 4. Comparison of the diffusivity in the space of micropores (probed with ethane; triangles) and mesopores (cyclohexane; circles) of the mesoporous zeolite NaCaA at room temperature. Given, for comparison, are also the diffusivities of ethane in the purely microporous zeolite and of cyclohexane in the neat liquid. The lines are shown to guide the eye.

Fig. 4 illustrates that the presence of the mesopores leads to a remarkable decrease in the intracrystalline diffusivities if – as provoked in the given experiments – the mesopores are excluded from mass transfer. For rationalizing the significance of this finding we quote the relation correlating the diffusivity in a medium with parallel, regularly arranged impermeable cylinders (D_{eff}, defined by Eq. (3) for sufficiently large displacements perpendicular to the cylinder axes) with the genuine diffusivity in the medium (D) [49]

$$\frac{D_{eff}}{D} = \frac{1-\phi}{1+\phi} \tag{14}$$

where ϕ denotes the volume fraction of the obstacles. Assuming a mass density of about 2 g/cm^3 for the purely microporous zeolite NaCaA, the volume fractions of the mesopores in NaCaA-2 and -5 result to be $\phi = 0.18$ and 0.30, respectively. With these numbers, Eq. (14) predicts diffusivity reductions by only about 30% in NaCaA-2 and 50% in NaCaA-5 in comparison with the purely microporous sample. The real drop in the diffusivities, namely by factors of about 5 to 10 as revealed by Figs. 3 and 4, is in striking contrast with this estimate and decidedly indicates that the space occupied by the mesopores is in no way adequately reflected by the model assumptions leading to Eq. (14). For giving rise to the observed dramatic reduction in the diffusivities, the mesopores must rather be assumed to be preferentially arranged in parallel layers, most likely – as suggested by the SEM images shown in Fig. 1 – as {100}, {010} and {001} planes. The parallel arrangement of diffusion inhibitors is an approved technology in the fabrication of polymer packing foils where the incorporation of aligned flakes is known to lead to significantly reduced permeation rates [54].

4. Conclusions

We have performed PFG NMR self-diffusion measurements with mesoporous zeolites of type NaCaA. By applying probe molecules of different size, by temperature variation and by a deliberate blockage of the mesopores we were able to vary the significance and the contributions of the different parts of the pore system to the observed overall mass transport. In this way, we determined a "hierarchy" of diffusivities by which it became possible to reflect different aspects of mass transfer in the pore space hierarchy. For enabling the direct measurement of these transport phenomena, the experiments had to be performed with relatively large crystals and at sufficiently low temperatures, i.e. under conditions which

deviate from those of the usual technological use of nanoporous materials. Correspondingly, the focus of our studies was directed on the exploration of transport phenomena in hierarchical pore systems quite in general rather than on a particular system and/or process.

In addition to confirming the efficiency of the mesopores for accelerating intracrystalline mass transfer and for providing, in this way, the basis for further performance enhancement in heterogeneous catalysis and mass separation, it was also possible to show that, if inhibited from mass exchange with the micropores, the presence of the mesopores may as well lead to a pronounced decrease in the intracrystalline diffusivities. If, during the technological application of such materials, coke depositions do lead to such blockages with increasing time on stream, the benefit of the mesopores gets lost and may, eventually, be even converted into its opposite.

The option to measure mass transfer separately in the micro- and mesopore spaces offers new prospects for the investigation of materials with hierarchical pore structure and for their optimized fabrication. Simultaneously with such studies of immediately technological relevance they do concern also the quite general question under which conditions and up to which extent mass transfer in complementary spaces can be correlated with each other. Both theoretical and experimental studies dedicated to this question are in preparation.

Acknowledgement

We dedicate this paper to Jens Weitkamp on the occasion of his 70th birthday, in appreciation of his activities for the zeolite community quite in general and, in particular, for a long-standing fruitful cooperation between his group in Stuttgart and the Leipzig group which has notably contributed to the developments in diffusion measurement, including the studies presented in this paper. We are obliged to the National Honor Scientist Program of the Ministry of Education, Science and Technology in Korea and the German Research Foundation for financial support and to Armin Bunde for directing our attention to diffusion phenomena in complementary pore spaces which were in the center of this study.

References

[1] F. Schüth, K.S.W. Sing, J. Weitkamp, Handbook of Porous Solids, Wiley-VCH, Weinheim, 2002.
[2] G. Ertl, H. Knözinger, F. Schüth, J. Weitkamp, Handbook of Heterogeneous Catalysis, second Edn., Wiley-VCH, Weinheim, 2008.
[3] J. Weitkamp, Solid State Ionics 131 (2000) 175.
[4] J. Weitkamp, L. Puppe, Catalysis and Zeolites, Springer, Berlin Heidelberg, 1999.
[5] F.J. Keil, R. Krishna, M.O. Coppens, Rev. Chem. Eng. 16 (2000) 71.
[6] R. Krishna, J. Phys. Chem. C 113 (2009) 19756.
[7] H. Jobic, D. Theodorou, Microporous Mesoporous Mater. 102 (2007) 21.
[8] J. Kärger, D.M. Ruthven, D.N. Theodorou, Diffusion in Nanoporous Materials, Wiley-VCH, Weinheim, 2012.
[9] N.Y. Chen, T.F. Degnan, C.M. Smith, Molecular Transport and Reaction in Zeolites, VCH, New York, 1994.
[10] J. Perez-Ramirez, D. Verboekend, A. Bonilla, S. Abello, Adv. Funct. Mater. 19 (2009) 3972.
[11] W. Fan, M.A. Snyder, S. Kumar, P.-S. Lee, W.C. Yoo, A.V. McCormick, R.L. Penn, A. Stein, M. Tsapatsis, Nat. Mater. 7 (2008) 984.
[12] M. Choi, H.S. Cho, R. Srivastava, C. Venkatesan, D.H. Choi, R. Ryoo, Nat. Mater. 5 (2006) 718.
[13] G. Wang, T.J. Pinnavaia, Angew. Chem. Int. Ed. 45 (2006) 7603.
[14] K. Na, C. Jo, J. Kim, K. Cho, J. Jung, Y. Seo, R.J. Messinger, B.F. Chmelka, R. Ryoo, Science 333 (2011) 328.
[15] A. Inayat, I. Knoke, E. Spiecker, W. Schwieger, Angew. Chem. Int. Ed. 51 (2012) 1962.
[16] J.C. Groen, L.A.A. Peffer, J.A. Moulijn, J. Perez-Ramirez, Chem. Eur. J. 11 (2005) 4983.
[17] J. Perez-Ramirez, S. Mitchell, D. Verboekend, M. Milina, N.L. Michels, F. Krumeich, N. Marti, M. Erdmann, ChemCatChem 3 (2011) 1731.
[18] D. Verboekend, J. Perez-Ramirez, Chem. Eur. J. 17 (2011) 1137.
[19] J. Kärger, Ind. Eng. Chem. Res. 41 (2002) 3335.
[20] D.M. Ruthven, in: H.G. Karge, J. Weitkamp (Eds.), Adsorption and Diffusion, Springer, Berlin, Heidelberg, 2008, p. 1.
[21] H. Jobic, in: H.G. Karge, J. Weitkamp (Eds.), Adsorption and Diffusion, Springer, Berlin, Heidelberg, 2008, p. 207.
[22] J. Kärger, in: H.G. Karge, J. Weitkamp (Eds.), Adsorption and Diffusion, Springer, Berlin, Heidelberg, 2008, p. 85.
[23] J. Kärger, R. Valiullin, in: R.K. Harris, R.E. Wasylishen (Eds.), Encyclopedia of Magnetic Resonance, John Wiley, Chichester, 2011. doi: 10.1002/9780470034590.emrstm0121.pub2.
[24] C. Chmelik, J. Kärger, Chem. Soc. Rev. 39 (2010) 4864.
[25] A. Feldhoff, J. Caro, H. Jobic, C.B. Krause, P. Galvosas, J. Kärger, ChemPhysChem 10 (2009) 2429.
[26] C. Chmelik, D. Enke, P. Galvosas, O.C. Gobin, A. Jentys, H. Jobic, J. Kärger, C. Krause, J. Kullmann, J.A. Lercher, S. Naumov, D.M. Ruthven, T. Titze, ChemPhysChem 12 (2011) 1130.
[27] J.C. Groen, W. Zhu, S. Brouwer, S.J. Huynink, F. Kapteijn, J.A. Moulijn, J. Perez-Ramirez, J. Am. Chem. Soc. 129 (2007) 355.
[28] R. Valiullin, J. Kärger, K. Cho, M. Choi, R. Ryoo, Microporous Mesoporous Mater. 142 (2011) 236.
[29] D. Mehlhorn, R. Valiullin, J. Kärger, K. Cho, R. Ryoo, ChemPhysChem 13 (2012) 1495.
[30] D. Mehlhorn, R. Valiullin, J. Kärger, K. Cho, R. Ryoo, Materials (open access) 5 (2012) 699.
[31] K. Cho, H.S. Cho, L.C. de Menorval, R. Ryoo, Chem. Mater. 21 (2009) 5664.
[32] W.S. Price, NMR Studies of Translational Motion, University Press, Cambridge, 2009.
[33] P.T. Callaghan, Translational Dynamics and Magnetic Resonance, Oxford Univ. Press, Oxford, 2011.
[34] J. Kärger, W. Heink, J. Magn. Reson. 51 (1983) 1.
[35] J. Kärger, Leipzig, Leipziger Universitätsverlag, Leipzig, Einstein Diffusion, 2010.
[36] A. Bunde, S. Havlin, Fractals and Disordered Systems, Springer, Berlin, 1996.
[37] J. Kärger, H. Spindler, J. Am. Chem. Soc. 113 (1991) 7571–7574.
[38] J. Kärger, Single-file Diffusion in Zeolites, in: H.G. Karge, J. Weitkamp (Eds.), Science and Technology – Molecular Sieves. vol. 7: Adsorption and Diffusion, Springer, Berlin Heidelberg, 2008, pp. 329–366.
[39] J. Michaelis, C. Bräuchle, Chem. Soc. Rev. 39 (2010) 4731.
[40] R.M. Cotts, M.J.R. Hoch, T. Sun, J.T. Markert, J. Magn. Reson. 83 (1989) 252.
[41] P. Galvosas, F. Stallmach, G. Seiffert, J. Kärger, U. Kaess, G. Majer, J. Magn. Reson. 151 (2001) 260.
[42] F. Stallmach, P. Galvosas, Annu. Rep. NMR Spectrosc. 61 (2007) 51.
[43] W. Heink, J. Kärger, H. Pfeifer, K.P. Datema, A.K. Nowak, J. Chem. Soc., Faraday Trans. 88 (1992) 3505.
[44] R. Valiullin, J. Kärger, Chem. Ing. Tech. 83 (2011) 166.
[45] D.M. Ruthven, W. DeSisto, S. Higgins, Chem. Eng. Sci. 64 (2009) 3201.
[46] J.H. Petropoulos, K.G. Papadokostaki, Chem. Eng. Sci. 68 (2012) 392.
[47] C.N. Satterfield, Mass Transfer in Heterogeneous Catalysis, M.I.T. Press, Cambridge, Massachusetts and London, England, 1970.
[48] V.N. Burganos, J. Chem. Phys. 109 (1998) 6772.
[49] E.L. Cussler, Diffusion: Mass Transfer in Fluid Systems, Cambridge University Press, Cambridge, 2009.
[50] D.M. Ruthven, K.F. Loughlin, J. Chem. Soc., Faraday Trans. I (68) (1972) 696.
[51] P. Zeigermann, S. Naumov, S. Mascotto, J. Kärger, B.M. Smarsly, R. Valiullin, Langmuir 28 (2012) 3621.
[52] J. Crank, The Mathematics of Diffusion, Clarendon Press, Oxford, 1975.
[53] D.W. McCall, D.C. Douglass, E.W. Anderson, J. Chem. Phys. 31 (1959) 1555.
[54] E.L. Cussler, in: S. Brandani, C. Chmelik, J. Kärger, R. Volpe (Eds.), Diffusion Fundamentals II, Leipziger Universitätsverlag, Leipzig, 2007, p. 324.